Review | Received 9 December 2025; Revised 10 May 2026; Accepted 11 May 2026; Published 12 June 2026
https://doi.org/10.55092/esp20260003

# Magnetic tunnel junctions for neuromorphic computing: from device physics to network architectures

**Liyuan Yang[1,2], Mengchun Pan[1,2], Peisen Li[1,2], Miaosen Liu[1,2] and Minhui Ji[3,*]**

[1] College of Intelligence Science and Technology, National University of Defense Technology, Changsha, China
[2] National Key Laboratory of Equipment State Sensing and Smart Support, National University of Defense Technology, Changsha, China
[3] The State Key Laboratory of Oral & Maxillofacial Reconstruction and Regeneration, National Clinical Research Center for Oral Diseases, Shaanxi Engineering Research Center for Dental Materials and Advanced Manufacture, Digital Center, School of Stomatology, The Fourth Military Medical University, Xi'an, China

* Correspondence author; E-mail: minhuiji109@163.com.

## Highlights:

- MTJ-based neuromorphic hardware.
- Potential applications in artificial intelligence.

**Abstract:** Neuromorphic computing is one of the most promising technologies to solve the Von Neumann bottleneck, which has the advantages of fast processing speed and low energy consumption in performing complex tasks. The development of neuromorphic computing is currently driven by several kinds of novel devices. Magnetic tunnel junctions (MTJs) are rich in nonlinear properties and can be regulated by multiple physical fields such as magnetic field, current and temperature. Meanwhile, MTJ has the advantages of good stability and low power consumption, which makes it an ideal device for neuromorphic computing. This paper starts by examining individual MTJ devices and then extends the discussion to full neural networks. First of all, we sorted out the various properties of MTJ, from the structure to physical mechanism and response characteristics. Secondly, the biological neuron model, synaptic properties and related studies on simulating neurons and synapses based on MTJs are introduced. Then, we review the neural network system-level architectures that have been explored with MTJ devices. Finally, the challenges and the future development trend are summarized for advancing MTJ-enabled neuromorphic computing.

**Keywords:** magnetic tunnel junctions; neuromorphic computing; neural networks

## 1. Introduction

In recent years, with the rapid development of the Internet of Things, Big Data, and Artificial Intelligence (AI) technologies, the volume of data collected by sensors has experienced explosive growth. Processing and storing such massive datasets pose major challenges to Von Neumann architecture-based computers: sharing a bus but suffering from performance mismatch, the computing and storage units exhibit high memory access latency and low computational efficiency (the "memory wall"), while data transfers between them during AI algorithm computation consume substantial energy (the "power wall"). These two issues have become key constraints on the further improvement of AI systems' intelligence level and computation ability. For example, although ChatGPT-4 demonstrates significant advantages in text understanding, text generation, and code writing, its vast parameter scale (estimated by recent academic analyses to be approximately 1.5 trillion parameters [1]) necessitates the use of tens of thousands of state-of-the-art graphics processing units for accelerated computation, with each inference consuming substantial energy. However, the human brain not only has powerful computing ability, but also consumes very little energy. According to calculations, when performing the same task, the brain's power consumption is estimated to be only 20 W [2], which is much lower than the computing power consumption of current computers. Therefore, rebuilding a new computing architecture (brain-like computing architecture) by simulating the computing methods of the human brain is expected to solve the current computing energy efficiency problem.

The brain-like computing architecture aims to realize neuromorphic computing by simulating the mechanisms of neurons and synapses that make up the human brain. Building hardware neuromorphic devices that can simulate the functions of neurons and synapses has become the key to realizing neuromorphic computing. Many companies and research institutions have conducted research on neuromorphic devices, such as IBM's TrueNorth [3] and Stanford University's Neurogrid chips [4]. Both integrate millions of neurons and billions of synapses made from Complementary Metal Oxide Semiconductor (CMOS) devices, and based on this, the neural networks are constructed. In training and computation of neural networks of the same scale, their energy consumption is lower compared to traditional computing chips. With the difficulty of improving semiconductor manufacturing processes and Moore's Law gradually reaching its limits, researchers hope to find better solutions by exploring new materials and new devices. Among them, new devices such as memristors [5], phase change devices [6], ferroelectric devices [7] and spintronic devices [8] have attracted widespread attention. The magnetic tunnel junctions (MTJs), the representative spintronic devices, have been regarded as one of the potential directions for realizing hardware neuromorphic computing, thanks to the advantages of clear mechanism, strong nonlinearity, low energy consumption, strong durability, mature stable fabrication process, and compatibility with CMOS.

MTJs have undergone three generations of device evolution, based on magnetic field control, spin-transfer torque (STT), and spin-orbit torque (SOT) modulation, respectively. Through material optimization and structural design, they have achieved remarkable progress in memory and magnetic sensor applications. At present, MTJs have advanced from fundamental laboratory research to large-scale industrial applications. Endowed with diverse modulation methods and intrinsic physical properties, MTJs can simulate the behaviors of neurons and synapses to construct neuromorphic devices, which can realize diversified functions in various computing architectures. This paper summarizes the recent

research progress on MTJ-based neuromorphic computing, analyzes the advantages and limitations of developing neuromorphic computing using MTJs, and finally proposes key issues that require further research and exploration in the future.

## 2. MTJ device physics

The core structure of an MTJ is a sandwich configuration consisting of two ferromagnetic layers and an intermediate nanoscale insulating layer. Electrons traverse this ultra-thin barrier layer (*i.e.*, the intermediate insulating layer) via the tunneling effect. When the relative orientation of the two ferromagnetic layers changes, the tunneling magnetoresistance of the MTJ varies accordingly—the phenomenon known as Tunneling Magnetoresistance (TMR). This effect was first discovered by French scientist Julliere in 1975, who also proposed a phenomenological model to explain it [9]. In 1989, Slonczewski updated this model [10] by incorporating a more accurate interpretation of the TMR effect. Taking an in-plane magnetized MTJ as an example, its schematic structure is shown in Figure 1a, where the arrows indicate the magnetic moment orientations of the ferromagnetic layers: the magnetic moment orientation of the reference layer is fixed (fixed layer), the intermediate barrier layer is made of a non-magnetic material, and the magnetic moment of the free layer can be switched under the regulation of an external magnetic field. The resistance of the device is determined by the angle $\theta$ between the magnetic moment orientations of the reference layer and the free layer. According to the model proposed by Slonczewski, the conductance of the device can be expressed as:

$$G = G_0(1 + P_1 P_2 \cos\theta) \tag{1}$$

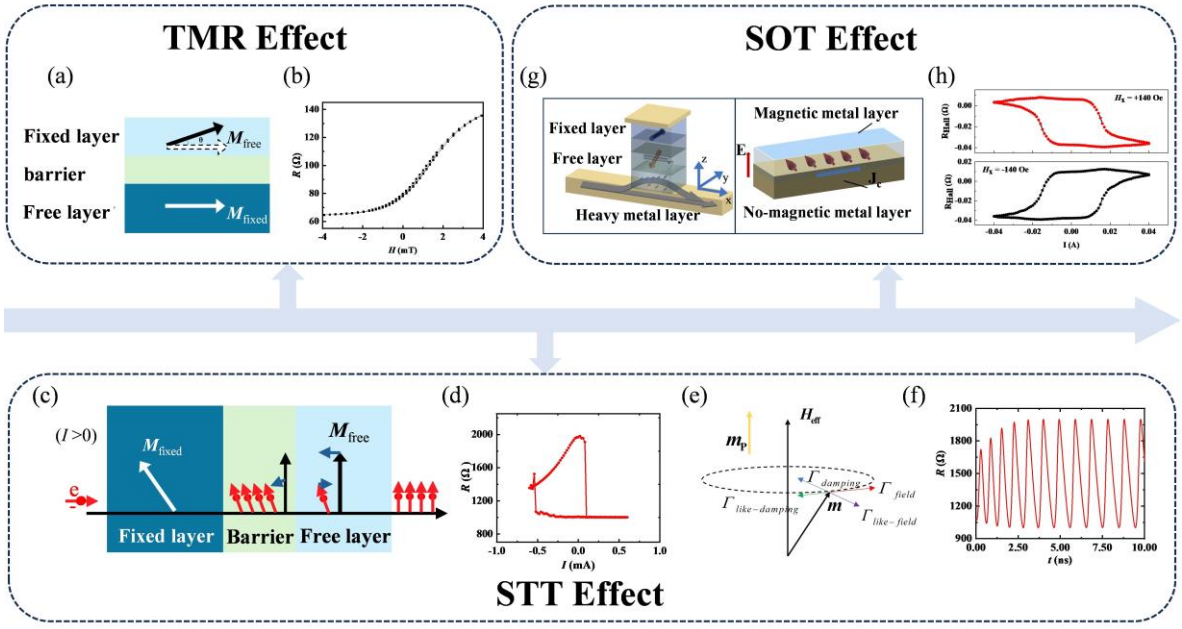


**Figure 1.** Different control methods for MTJs. **(a)** Schematic of in-plane magnetized MTJ Structure; **(b)** Tunneling magnetoresistive test curve of MTJ; **(c)** Schematic diagram of the STT effect principle; **(d)** MTJ resistance switching curve driven by STT; **(e)** Schematic diagram of the torque on magnetic moment in free layer of a STT-MTJ; **(f)** STNO resistance oscillation time-domain response curve; **(g)** Schematic of spin Hall effect and Rashba-Edelstein effect; **(h)** Hall resistance variation curve driven by the SOT effect.

In the formula, $G_0$ represents the average surface conductance of the magnetic multilayer film, $P_1$ and $P_2$ represent the effective spin polarization rates from the two ferromagnetic layers to the barrier layer respectively. The response curve is shown as Figure 1b. According to Formula (1), when the magnetic moments of the free layer and the reference layer are parallel, the MTJ is in a low resistance state, represented by $R_p$; when the magnetic moments of the two ferromagnetic layers are antiparallel, the MTJ resistance value is the highest, represented by $R_{ap}$. At this time, the magnetoresistance change rate of the tunnel junction can be expressed as follows:

$$TMR = (R_{ap} - R_p) / R_p \times 100\% \tag{2}$$

In 1996, American physicists Slonczewski and Berger theoretically proposed the current-induced magnetic moment switching effect [11], known as STT effect. In an MTJ, when a current is injected, spin-polarized electrons carry spin angular momentum and transfer it to the free layer, thereby reorientating the free layer's magnetic moment and modulating the junction's magnetoresistance. Taking the current-perpendicular-to-plane (CPP) structure (the current flows perpendicular to the junction plane) as an example (Figure 1c): when current flowing from the free layer to the reference layer, electrons drift from the reference layer to the free layer. Since the reference layer's magnetic moment is pinned in a fixed direction, electrons become spin-polarized as they pass through the reference layer, adopting the same spin orientation as the reference layer's magnetization. These spin-polarized electrons then tunnel into the free layer. During scattering with the free layer's magnetic moment, a portion of the spin angular momentum from the polarized electrons is transferred to the free layer's magnetic moment, which is equivalent to exerting an effective torque on it. The influence of spin-polarized current on the magnetic moment can be described by the Landau-Lifshitz-Gilbert-Slonczewski (LLGS) equation [12]:

$$\begin{cases} \boldsymbol{dm}/\boldsymbol{dt} = \Gamma_{\text{field}} + \Gamma_{\text{damping}} + \Gamma_{\text{like-damping}} + \Gamma_{\text{like-field}} \\ \Gamma_{\text{field}} = -\gamma \boldsymbol{m} \times \boldsymbol{H}_{eff} \\ \Gamma_{\text{damping}} = \gamma\alpha \boldsymbol{m} \times \left(\boldsymbol{dm}/\boldsymbol{dt}\right) \\ \Gamma_{\text{like-damping}} = \gamma\alpha_J \boldsymbol{m} \times \left(\boldsymbol{m} \times \boldsymbol{m}_{\mathbf{p}}\right) \\ \Gamma_{\text{like-field}} = \gamma \boldsymbol{b}_J \boldsymbol{m} \times \boldsymbol{m}_{\mathbf{p}} \end{cases} \tag{3}$$

In the formula, $\boldsymbol{m}$ is the normalized vector of the free layer magnetic moment, $\boldsymbol{m}_{\mathbf{p}}$ is the normalized vector of the reference layer magnetic moment, $\gamma$ is the gyromagnetic ratio, $\alpha$ is the magnetic damping coefficient, and $\alpha_J = gJ\hbar / 2e\boldsymbol{M}_{\mathbf{S}}h\mu_0$ is the spin transfer torque coefficient (where $g$ is the spin transfer factor, $J$ is the current density through the free layer, $\hbar$ is the reduced Planck constant, $e$ is the electron charge, $\boldsymbol{M}_{\mathbf{S}}$ is the saturation magnetization of the free layer magnetic moment, $h$ is the thickness of the free layer, $\mu_0$ is the permeability of free space), $b_J = \beta\alpha_J$ is the field-like moment coefficient, $\beta$ represents the ratio of spin moment to field-like moment, and $\boldsymbol{H}_{\mathbf{eff}}$ is the effective field, which includes various fields such as anisotropic fields, external magnetic fields, demagnetizing fields, thermal effect fields, and exchange fields. $\Gamma_{\text{field}}$ is the precession term, $\Gamma_{\text{damping}}$ is the damping term, $\Gamma_{\text{like-damping}}$ is the spin transfer torque brought by the STT effect, and $\Gamma_{\text{like-field}}$ is the field-like torque brought by the STT effect.

The magnetoresistance change of the MTJ driven by external current is shown in Figure 1d. By analyzing the direction and magnitude of the torque on the free layer magnetization, the magnetoresistance

state of the junction can be obtained. Figure 1e shows the situation in which the effective field of the MTJ is aligned with the reference-layer magnetization. By analyzing the direction and magnitude of the torque exerted on the free layer magnetic moment, the motion state of the free layer magnetic moment can be obtained.

Under the STT effect, when the STT and the damping torque are equal in magnitude and opposite in direction, they can cause the magnetization of the free layer to undergo steady precession, manifesting as a regular oscillation in the magnetoresistance of the MTJ as shown in Figure 1f. On the one hand, this new type of microwave oscillator is called a Spin Transfer Nano-Oscillator (STNO), which can generate microwave signals from 1 to 100 GHz and can be used for microwave emission [13]. On the other hand, when a microwave signal is injected into STNO, the device will output a DC voltage signal under the spin ferromagnetic resonance and magnetoresistance effects. Because the output response is similar to the diode rectification effect, it is called the Spin Torque Diode (STD) effect. This effect provides a physical basis for realizing microwave detection. In addition, among multiple STNO devices, the device oscillation is affected by the oscillation of other connected devices, thereby realizing the multi-device coupling.

Thermal fluctuations impose fundamental limits on the thermal stability of MTJs, inducing random perturbations in the magnetization direction that manifest as stochastic noise in the magnetoresistance signal. The parallel (P) and antiparallel (AP) states, corresponding to energy minima in the magnetic free-energy landscape, are separated by an energy barrier $\Delta E$. Thermally activated crossing of this barrier leads to stochastic switching between the two resistance states. According to the Néel–Brown theory [14], the mean residence time $\tau_{P/AP}$ in each state follows an Arrhenius-type law. Notably, in practical perpendicular MTJ (p-MTJ) devices, the P and AP states exhibit inherent asymmetry: this asymmetry arises from non-idealities at the structural level (e.g., interface roughness, thickness variations) and material level (e.g., differences in damping constants and magnetic anisotropy), which directly lead to distinct energy depths and transition rates between the two states, further modulating the stochastic dynamics of the device. When the thermal stability factor $\Delta = \Delta E / k_B T$ approaches or falls below unity, the energy barrier is comparable to the thermal energy $k_B T$. In this regime, thermal fluctuations induce frequent and random magnetization flips, placing the device into the superparamagnetic regime. Such superparamagnetic tunnel junctions exhibit ultrafast stochastic dynamics, which are governed by the relaxation time:

$$\frac{1}{\tau_{P/AP}} = \phi_0 \exp\left[-\frac{\Delta E_0}{k_B T}\left(1 \pm \frac{I}{I_C}\right)\right] \tag{4}$$

where $\phi_0$ is the attempt frequency (related to the device's flipping mechanism), $k_B$ is Boltzmann's constant, $T$ is the ambient temperature.

To modulate stochastic switching for neuromorphic applications, STT is typically employed to manipulate the energy barrier. A common approximation for the current-dependent barrier height is $\Delta E(I) = \Delta E_0(1 \pm I / I_C)$, where the sign convention reflects the assisting or hindering effect of the applied current $I$ on the switching process [15]. Substituting this into Equation (4) yields the state-dependent residence times. Based on this statistical description, the probability that the MTJ remains in a given state after a sampling time $\Delta t$ is $P(\text{stay}) = \exp(-\Delta t / \tau_{P/AP})$. Consequently, the switching probability within $\Delta t$ is given by:

$$P_{\text{switch}} = 1 - \exp\left(-\frac{\Delta t}{\tau_{\text{P/AP}}}\right) \quad (5)$$

highlighting the stochastic nature of MTJ switching, which is a critical consideration for both reliable memory operation and probabilistic computing implementations.

The STT effect relies heavily on the direct transfer of spin angular momentum from conduction electrons to the local magnetic moment, and is constrained by the inherent "read-write shared vertical current path" design. This approach inevitably faces bottlenecks such as high critical current density, elevated write power consumption, and limited device endurance. Furthermore, the magnetic moment switching speed is restricted by the intrinsic precession dynamics. SOT utilizes a spin current generated via spin-orbit coupling to manipulate the magnetic moment state, arising from a combination of the spin Hall effect (SHE) and the interface Rashba-Edelstein effect. The spin Hall effect refers to the phenomenon where, under a longitudinal charge current (e.g., along the x-direction) in a non-magnetic heavy metal layer, electrons with opposite spin orientations experience transverse deflection (along the $\pm$y-direction), resulting in spin accumulation at the transverse boundaries (y-direction) with spin polarization oriented perpendicularly (along the z-direction), thereby generating a pure spin current flowing along the transverse direction. The interface Rashba-Edelstein effect arises from structural inversion asymmetry at the interface between a ferromagnetic layer and a non-magnetic heavy metal layer. This broken inversion symmetry generates a built-in electric field perpendicular to the interface (along the z-direction). When a charge current flows in-plane (along the x-direction), this electric field, combined with spin-orbit coupling, produces an effective magnetic field that induces a non-equilibrium spin accumulation at the interface. Crucially, this spin accumulation is oriented transversely (along the $\pm$y-direction). Under the influence of this interfacial spin accumulation, the adjacent free layer experiences a spin-orbit torque that drives magnetic moment switching, as illustrated in Figure 1g. The dynamic process of SOT-induced magnetization switching can be described by the following modified Landau-Lifshitz-Gilbert equation including spin-orbit torque terms:

$$d\boldsymbol{m}/dt = \Gamma_{\text{field}} + \Gamma_{\text{damping}} + \Gamma_{\text{SOT-damping}} + \Gamma_{\text{sot-field}} \quad (6)$$

In the formula, $\Gamma_{\text{SOT-damping}}$ is the damping-like torque brought by the SOT effect, and $\Gamma_{\text{SOT-field}}$ is the field-like torque brought by the SOT effect. Similar to the STT effect, SOT can also cause magnetic moment oscillation.

To facilitate reading and comprehension of the theoretical derivations, model analyses, and simulation results throughout this paper, a unified definition of the frequently used physical symbols is provided below. Table 1 systematically lists the key symbols involved in this work, including their corresponding physical meanings, standard international units, and core application scenarios in MTJs, magnetization dynamics, and neuromorphic computing models.

**Table 1.** List of symbols, physical meanings, units, and core application scenarios in this paper.

| Symbol | Physical Meaning | Unit | Core Application Scenario |
|---|---|---|---|
| $G_0$ | Average surface conductance of magnetic multilayer film | S (Siemens) | TMR conductance calculation |
| $P_1$, $P_2$ | Effective spin polarization rate of two ferromagnetic layers to barrier layer | Dimensionless | TMR effect conductance model |
| $\theta$ | Angle between magnetic moment orientations of reference layer and free layer | rad (radian) | MTJ resistance state determination |
| $R_p$ | Low resistance state of MTJ (parallel magnetic moments) | Ω (Ohm) | MTJ resistance state characterization |
| $R_{ap}$ | High resistance state of MTJ (antiparallel magnetic moments) | Ω (Ohm) | MTJ resistance state characterization |
| $\boldsymbol{m}$ | The normalized vector of the free layer magnetic moment | Dimensionless | STT/SOT magnetization dynamics |
| $\boldsymbol{m_p}$ | The normalized vector of the reference layer magnetic moment | Dimensionless | STT/SOT magnetization dynamics |
| $\gamma$ | Gyromagnetic ratio | rad · $s^{-1}$ · $T^{-1}$ | Landau-Lifshitz-Gilbert (LLG) equation |
| $J$ | Current density through free layer | A/m ²(Ampere per square meter) | STT effect torque calculation |
| $\hbar$ | Reduced Planck constant | J s (Joule second) | Quantum spin dynamics calculation |
| $e$ | Elementary charge | C (Coulomb) | Spin current and torque calculation |
| $\boldsymbol{M_S}$ | Saturation magnetization of free layer | A/m (Ampere per meter) | STT torque coefficient calculation |
| $h$ | Thickness of free layer | m (meter) | STT torque coefficient calculation |
| $\mu_0$ | Permeability of free space | H/m (Henry per meter) | Magnetic field and torque calculation |
| $\beta$ | Ratio of spin moment to field-like moment | Dimensionless | STT effect torque decomposition |
| $\boldsymbol{H_{eff}}$ | Effective magnetic field (anisotropic, external, demagnetizing, *etc.*) | A/m (Ampere per meter) | Magnetization dynamics of free layer |
| $\Delta E$ | Barrier energy for magnetic moment flipping | J (Joule) | Néel-Brown relaxation theory |
| $k_B$ | Boltzmann's constant | J/K (Joule per Kelvin) | Thermal fluctuation and superparamagnetism |
| $T$ | Ambient temperature | K (Kelvin) | Thermal effect on MTJ magnetization |
| $I_C$ | Critical current for MTJ magnetic moment flipping | A (Ampere) | STT/SOT switching threshold |
| $I$ | Current flowing through MTJ | A (Ampere) | MTJ switching control and probability calculation |
| $\Delta t$ | Sampling time | s (second) | Néel-Brown relaxation probability calculation |
| $w_i$ | Synaptic weight | Dimensionless | Artificial neuron model (input weighting) |
| $x_i$ | Input signal | Dimensionless | Artificial neuron model |
| $b$ | Threshold of artificial neuron | Dimensionless | Artificial neuron activation judgment |

## 3. Spin neuromorphic device

The most basic information processing units in the human brain are neurons and synapses. The number of neurons in the human brain is on the order of $10^{11}$, and the number of synaptic connections between them reaches approximately $10^{15}$ [16]. Neurons are interconnected through synapses to form a complex

neural network. When a neuron receives information from other neurons or the external environment, this information will induce changes in the membrane potential of the neuron; subsequently, the neuron transmits the processed information to other neurons or target cells through synapses. The transmission and processing of these signals constitute the fundamental basis for the brain to perform information processing, enabling the brain to carry out complex information integration, analysis and decision-making, thereby maintaining the normal operation of human cognitive, emotional and social behavioral functions [17].

### *3.1. Synapse*

Synaptic neuromorphic devices mainly implement three core functions: memory storage (storing long-term or short-term memory in the form of weights), signal transmission (realizing the multiplication operation between input signals and weights), and plasticity (dynamically updating weights during network training). Different network architectures have significantly different performance requirements for synaptic devices. Artificial neural networks (ANNs) focus on high-precision weight storage, linear weight modulation and stable batch update capabilities to adapt to the backpropagation algorithm, which is the core algorithm of ANNs; spiking neural networks (SNNs), which are more bionic, emphasize precise timing response, biological plasticity mechanisms such as Spike-Timing-Dependent Plasticity (STDP), event-driven low-power consumption characteristics, and compatibility with short-term and long-term multi-scale information processing [18].

As a typical synaptic device, MTJ uses magnetization state mapping weights to achieve non-volatile storage, complete input and weight multiplication operations through resistance changes, and uses the STT/SOT effect to dynamically update weights. It has now reached nanosecond-level switching speeds, hundreds of picojoules of energy consumption, showing high energy efficiency advantages in scenarios such as pattern recognition. To address the issue that the inherent low-resistance characteristic of MRAM devices tends to induce excessive power consumption in conventional current-summation crossbar architectures, Jung *et al.* developed a 64 × 64 MRAM crossbar array based on the one-transistor-one-magnetic tunnel junction (1T-1MTJ) structure in 2022 [19], whose configuration is illustrated in Figure 2a. For the implementation of analog multiply-accumulate (MAC) operations, the research team proposed a resistance-summation-based architecture. By virtue of an XNOR gate, this architecture converts the basic multiplication between the input and weight in AI computing into a hardware-level operation, which is based on voltage-controlled path selection and resistance-state output: a high resistance is produced when the input and weight have the same value, whereas a low resistance is output when their values differ, and the result of this resistance variation is exactly equivalent to the product of the multiplication operation. Sixty-four such bit-cells were connected in series along a column, and the total resistance of the column is the sum of the resistance outputs from the XNOR gates of all bit-cells. This total resistance corresponds to the dot product of the input vector and the column weight vector, thereby accomplishing the accumulation step of the MAC operation. Finally, by leveraging the time-delay characteristic of capacitor charging by resistance, the resistance value is converted into a charging time, which is measured and digitized using a 4-bit time-to-digital converter (TDC). This approach enables the accurate reading of resistance values while satisfying the constraints on chip power consumption and area. However, this scheme still faces core challenges: first, the realization of high-precision in-memory computing requires compensation by expanding the neural network scale or prolonging the computing

time; second, analog noise accumulates continuously during column-wise resistance summation and may eventually exceed the least significant bit (LSB) resolution of the TDC, leading to the invalidation of computing results. In addition, magnetic crosstalk is prone to occur during the integration of large-scale arrays. Moreover, the 1T-1MTJ structure requires relatively large access transistors to ensure reliable read and write operations, which not only degrades the switching speed but also introduces current interference during read operations.

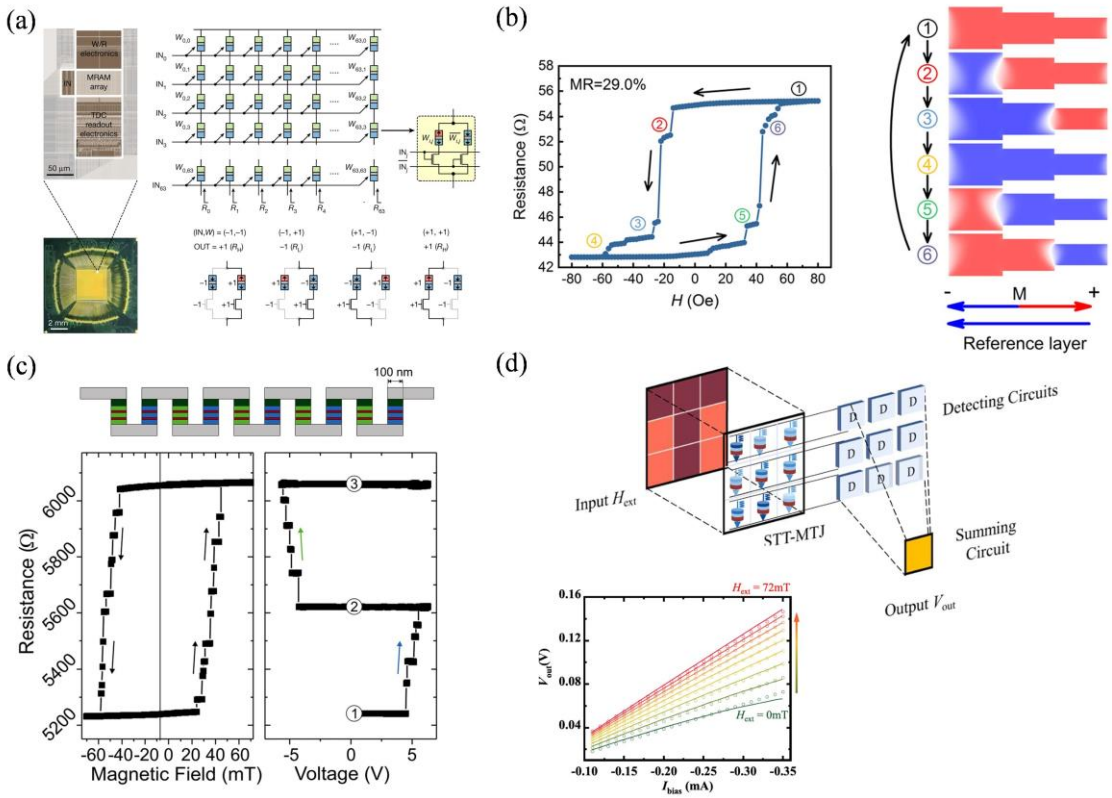


**Figure 2.** The non-volatile characteristic of MTJs mimics synaptic memory. **(a)** 1T-1MTJ MTJ unit and array [19]. Reprinted with permission. Copyright 2022 Nature; **(b)** Multi-domain synaptic devices [20]. Reprinted with permission. Copyright 2017 AIP Publishing; **(c)** Chain of MTJs as a synaptic device [21]. Reprinted with permission. Copyright 2018 AIP Publishing; **(d)** Nonlinear synapse by utilizing STNO [22]. Reprinted with permission. Copyright 2024 Elsevier.

Compared with binary MTJs that can only encode two discrete states, MTJs with memristive capabilities enable richer information representation and higher computational density. At present, the multi-state control capability is mainly achieved through the magnetic domain wall MTJ structure. In 2017, Cai *et al.* prepared MTJ strips with stepped width changes, and realized six resistance states by utilizing the multi-magnetic domain flipping that occurred during the magnetization flipping process of the MTJ [20], as shown in Figure 2b. MTJ devices based on magnetic domain wall motion can better simulate synaptic multi-valued plasticity. In 2018, Raymenants *et al.* connected 10 MTJs in series to exhibit multiple resistance states, and this state can be regulated by external magnetic fields and voltage pulses, thereby simulating the synaptic weight memory function [21], as shown in Figure 2c. Under the control of a magnetic field, the spin synapse of multiple devices in series exhibits multiple stable resistance states.

Most current research in the field of ANNs focuses on the development and application of linear synaptic devices, mainly because of their strong interpretability of weight modulation, easy compatibility with traditional backpropagation algorithms, and clear advantages in numerical calculation accuracy. However, linear synapses often require deeper network levels or more computing resources when processing complex nonlinear tasks, making it difficult to efficiently capture nonlinear correlations in data. Nonlinear synapses theoretically have better complex feature extraction and nonlinear mapping capabilities. In 2024, Ji *et al.* proposed the concept of a nonlinear synapse by exploiting the voltage-output nonlinearity during STNO oscillations [22], as shown in Figure 2d. They constructed a convolutional neural network to complete a letter recognition task. The nonlinear multiply-accumulate operation effectively improved the convergence speed, achieving a simulation accuracy of 100%. Compared with the linear synapse network, it not only accelerated the convergence speed but also improved the computational accuracy.

The MTJ flipping process has controllable nonlinearity. It can be used to simulate the STDP and short-term/long-term dual-scale plasticity of SNN, therefore it is suitable for SNN synaptic neuromorphic devices. In 2015, Sengupta *et al.* mapped the high-resistance state and low-resistance state of the MTJ to the memory and forgetting, respectively. The continuous change in resistance during the magnetization flipping process of the MTJ device can be used to simulate long and short-term plasticity [23], as shown in Figure 3a. When the MTJ flips from a low-resistance state to a high-resistance state, long-term memory is achieved. At the same time, studies have also proven that the amplitude, duration and frequency of input stimulation play a key role in the long-term potentiation properties of synapses.

The sensitivity of synapses can be modulated by optimizing the shape and size of the MTJ, enabling the simulation of biological forgetting processes. Synaptic plasticity includes STDP, facilitation, depression, potentiation, long-term potentiation (LTP) and long-term depression (LTD). In 2020, Prasad *et al.* constructed an MTJ synaptic device with short-term/long-term memory capability by injecting current to cause magnetic domain wall motion [24], as shown in Figure 3b. Moreover, Zhang *et al.* used an MTJ array with random flipping characteristics to simulate synaptic plasticity. They connected multiple p-MTJs with random characteristics in parallel to form a compound magnetoresistive synapse (CMS) [25], as shown in Figure 3c. Under the continuous amplitude and time control of programmable voltage pulses, this synapse can achieve LTP and LTD. Although this solution can improve the resolution of individual synaptic weights by increasing the number of integrated p-MTJs, this will lead to a reduction in the integration density of neuromorphic circuits, so a trade-off between resolution and integration is required. In 2023, Lone *et al.* used magnetic skyrmion devices to simulate the plasticity of biological synapses. As shown in Figure 3d, the region from point A to point B is partitioned into a presynaptic segment and a postsynaptic end, and the current was injected into the heavy metal layer of this structured device [26]. Since magnetic skyrmions are regulated by electric current, the Z-axis magnetization of the presynaptic segment and postsynaptic end changes due to their particulate behavior. Such characteristics can be exploited to emulate synaptic short-term plasticity, long-term plasticity, and STDP. In 2023, Cao *et al.* realized multiple simulated, non-volatile resistance states with enhanced linearity and symmetry in SOT devices, thereby generating programmable and stable synaptic weights, while verifying their synaptic plasticity such as LTP and LTD [27], as shown in Figure 3e. However, current research on synaptic plasticity of skyrmions is mostly based on simulation research.

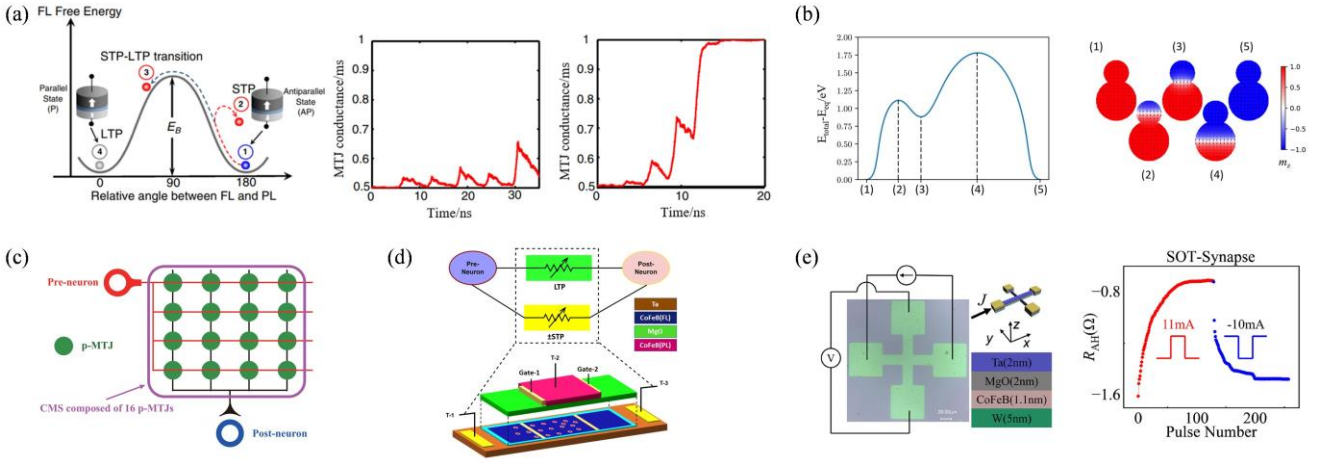


**Figure 3.** Modeling synaptic plasticity using the MTJ switching behavior. **(a)** Schematic diagram of the STT effect to control the transition between long-time-range plasticity and short-time-range plasticity [23]. Reprinted with permission. Copyright 2016 APS; **(b)** Synaptic devices based on magnetic domain wall motion [24]. Reprinted with permission. Copyright 2020 AIP Publishing; **(c)** a compound magnetoresistive synapse [25]. Reprinted with permission. Copyright 2016 ACM; **(d)** Synaptic devices based on magnetic skyrmion [26]. Reprinted with permission. Copyright 2023 IEEE; **(e)** SOT-based spiking synaptic device [27]. Reprinted with permission. Copyright 2023 IEEE.

### *3.2. Neuron*

Neurons are the basic units that constitute the structure of biological neural networks, and are also the basic units that form the cognitive behavior of the brain. There are many neuron models, which are mainly divided into two categories. One is the symbolic artificial neuron model, such as the M-P (McCulloch-Pitts) model; the other is the spiking neuron model, such as the H-H (Hodgkin-Huxley) model, IZ (Izhikevich) model, LIF (Leaky Integrate-and-Fire) model, *etc.*

The M-P neuron model was proposed by psychologist W. McCulloch and mathematician W. Pitts in 1943, and it has become a foundational abstraction for modern artificial neural networks. Its basic function can be expressed as a linear weighted sum of inputs and weights, and then it is given nonlinear characteristics through a nonlinear activation function. This process can be expressed as:

$$y = f(\sum_{1}^{N} w_i x_i - b) \tag{7}$$

In the formula: $w_i$ is the weight, $x_i$ is the input, $b$ is the bias, and $f$ is the nonlinear activation function.

The key to using the MTJ structure to build M-P neurons is to simulate two basic functions. The first is to realize the multiplication and summation of inputs and weights; the second is to realize the simulation of nonlinear activation functions. Recently, researchers have used the resistance change and random switching behavior of MTJs to simulate the nonlinear activation function (ReLU and sigmoid function) of neurons [27,28], and based on this, they have constructed a spin neural network with high accuracy and fast training speed.

Unlike M-P neurons, spiking neurons are more consistent with the signal transmission method in biological nervous systems. Because the LIF model can simulate the three basic characteristics of

biological neurons: leakage, integration, and excitation, it can meet the computing needs of spiking neural networks, and it has the advantage of simple calculation compared to other spiking neuron models and can be implemented in large-scale simulation systems. Therefore, most researchers choose the LIF neuron model for simulation. In the LIF model, a pulse will be emitted only when the input exceeds a fixed threshold. After the emission, the membrane potential will gradually decrease. In addition, a period of non-response area will appear after the pulse is emitted. The mathematical description of the model is:

$$C_1 \frac{dV_1}{dt} = -G_L(V_1 - E_L) + I_{in} \quad (8)$$

In the formula: $I_{in}$ is the input current, $C_1$ is the cell membrane surface capacitance, $G_L$ is the admittance during leakage, and $E_L$ is the balanced voltage. Parameters such as neuron firing rate, firing interval length, and minimum firing current can be calculated through this model.

Neuroscience has discovered that humans have a variety of neurons with different structures, which can achieve rich functions and can be divided into three categories: sensory neurons, motor neurons and interneurons [29]. Sensory neurons transmit the information code of the sensory cells inward, mainly realizing the pulse encoding of external information; motor neurons transmit information outward; interneurons carry out information transmission and calculation. By constructing LIF model neurons, the interneurons can be simulated to receive and integrate input pulses from other neurons, and send out their own pulses according to the intensity and frequency of these input pulses. The following is an introduction to related research on simulating sensory neurons and interneurons based on MTJs.

Sensory neurons encode various external stimulation signals and spread information in the nervous system in the form of nerve impulses to realize external perception [30]. By designing MTJ sensing neurons to mimic neural pulse coding, brain-like perception can be achieved while improving information-acquisition efficiency. In 2015, Suh *et al.* used the random flipping characteristics of MTJs to simulate the neural coding characteristics of neurons [31], as shown in Figure 4a. In the figure, $R_{NM}$ is an MTJ neuron device with random flipping characteristics, $R_{SM}$ is a magnetic memristor, $R_{L1}$ and $R_{L2}$ are both load resistors, and the turn-on voltage of transistor $T_0$ is set between $V_{ap}$ and $V_p$. A constant voltage smaller than the turn-on voltage of the transistor is applied to input terminal 1, and a changing magnetic field is applied to input terminal 2. The flipping probability of the MTJ is adjusted by changing the magnetic field. In addition, applying a pulse signal of the same frequency as the $R_{NM}$ to the $R_{SM}$ can also achieve the flipping of the $R_{SM}$. The change in device resistance caused by the flipping can be used to simulate the plasticity of synapses. This scheme simulates the coding function of incoming neurons and the plasticity of synapses.

A single neuron has a variety of coding methods, including frequency coding, time coding, pattern coding, *etc.* The difference lies in the different forms of expressing information. In the case of multi-stimulus input, neuron clusters release coding, which requires cluster synchronization of neurons. Neuron cluster coding regards the cell cluster composed of cells with simultaneous increase in firing rate as the basic unit for expressing information [32], which ensures flexible perception of the external environment while improving the robustness of the system. In 2022, Zhang *et al.* took advantage of the controllable random flipping characteristics of MTJs: one flipping of MTJ represents one pulse firing, and they changed the firing rate of MTJs by adjusting the input current

to perform population coding [33], the result is shown in Figure 4c. This kind of population coding can effectively solve the robustness problem caused by device non-uniformity, which is a key challenge in large-scale neuromorphic array integration.

In sensory neuron simulations, the random switching behavior and process change effects of MTJs will lead to additional stimulation time and related CMOS peripheral circuit design [34]. How to reduce additional stimulation and optimize peripheral circuits has become a problem to be solved in this direction. Constructing LIF model neurons can realize the simulation of interneurons. Researchers have proposed a variety of solutions, including using spin oscillators, multi-domain devices and magnetic skyrmion devices. In 2022, Marković *et al.* used Spin-Hall Nano-Oscillators (SHNOs) as a spiking neuron and proved through micromagnetic simulation that SHNO can generate voltage spikes to simulate biological neurons [35]. As shown in Figure 4b, a small current pulse is applied to spin neuron indicated by the dotted line, triggering a phase spike (red curve). The resulting spin excitations propagate through the exchange-coupled lattice and subsequently push another spin neuron over its threshold, inducing a delayed spike (blue curve). Secondly, the article proves that through the coupling between SHNOs, the information transfer between neurons can be simulated, and the pulse energy from two neurons in the same layer can be added and injected into the neurons of the next layer. This also provides a new direction for the development of large-scale neural networks.

In addition, researchers have taken advantage of the rich adjustability of MTJs to simulate neuron characteristics through multi-field coordination. In 2022, Wang *et al.* used the synergy of the SOT effect and the built-in field in the gradient magnetic anisotropic MTJ to control the movement of the magnetic domain wall [36], as shown in Figure 4d. This device simulated the LIF model of biological neurons, achieved self-resetting of neurons, reduced neuron integration/leakage time, and at the same time reduced the energy consumption of the device to simulate neurons. Experiments have verified that the integration/leakage time of this neuron can be as high as 12–15 ns, and the integration power consumption is 65 μW. In the same year, Wang *et al.* improved on the heavy metal SOT-MTJ device and designed a multi-particle composite free layer which achieved continuous changes in the resistance of the SOT device. It not only simulated the neuron pulse firing behavior, but also realized the integration of neuron membrane potential and the simulation of leakage characteristics [37]. In 2020, Yu *et al.* proposed an extremely low-power nanodevice composed of a piezoelectric substrate and synthetic antiferromagnetic skyrmions [38]. As shown in Figure 4e, a weak electric field is applied to the heterojunction to regulate the interface antiferromagnetic coupling, controlling the conversion of skyrmions from large to small to achieve changes in the resistance of the MTJ device. This feature is used to simulate the neuron LIF model, and also simulate the enhancement/inhibition characteristics of synapses, with an energy consumption of 0.3 fJ.

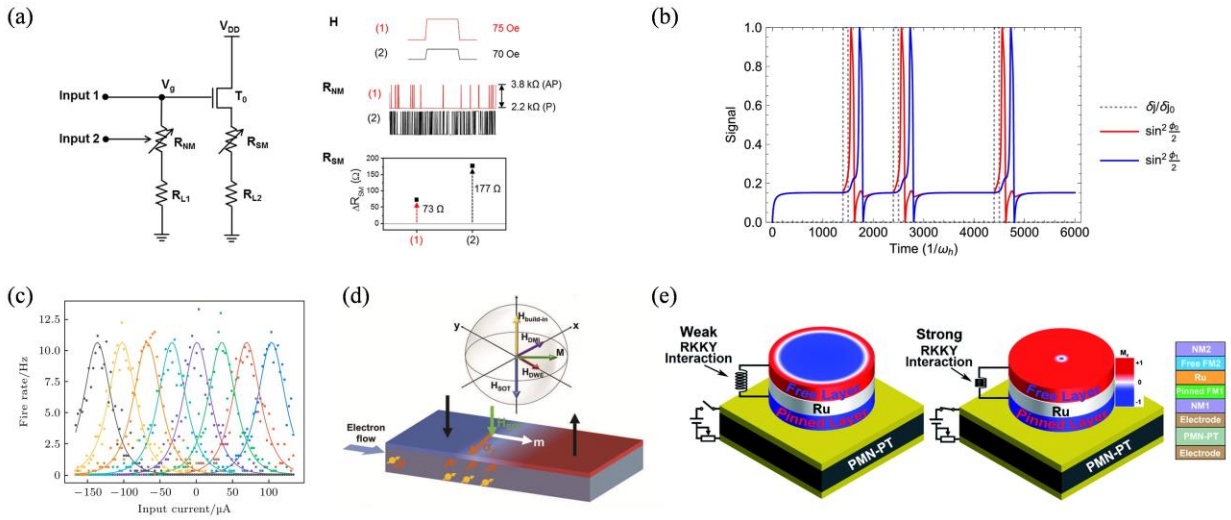


**Figure 4.** MTJ devices for simulating neuronal behavior. **(a)** Neuronal coding circuit and example of neuronal coding [31]. Reprinted with permission. Copyright 2015 AIP Publishing; **(b)** Impulse behavior of SHNO-based neurons and MTJ devices based on the SOT effect simulating the LIF neuron model [35]. Reprinted with permission. Copyright 2022 APS; **(c)** Neuronal population coding results based on stochastic switched MTJs [33]. Reprinted with permission. Copyright 2022 CPS; **(d)** Simulation of LIF neuron model for MTJ based on magnetic domain wall motion behavior [36]. Reprinted with permission. Copyright 2022 Wiley; **(e)** Synthetic antiferromagnetic skyrmion devices [38]. Reprinted with permission. Copyright 2020 RSC.

Table 2 summarizes the different functions of various devices used in neuromorphic computing. To summarize, MTJ-based neuromorphic devices leveraging STT, SOT, domain wall, and skyrmion effects exhibit distinct characteristics and complementary advantages in emulating synaptic and neuronal functions. Among them, STT-MTJs represent the most mature technological route to date. However, constrained by intrinsic write disturbance effects and their binary resistance states, they still face bottlenecks in achieving high-precision linear weight modulation and supporting high-speed, event-driven computing in SNNs [39]. In contrast, SOT-MTJs effectively mitigate write disturbance issues through decoupled read/write paths. Their ultra-fast switching speeds and linear LTP/LTD characteristics make them ideal candidates for constructing high-performance LIF spiking neurons, significantly advancing the development of low-power SNN systems [40]. Nevertheless, they must still overcome challenges such as thermal effects induced by high write currents and process integration complexities arising from intricate heavy-metal stacks [41]. Domain-wall MTJs, owing to their continuously tunable resistance state, provide a natural foundation for simulating the continuous plasticity of biological synapses, significantly enhancing weight resolution and information storage density. However, state instability and slow response times caused by domain wall pinning effects remain major obstacles to large-scale array integration [42]. Skyrmion MTJs, benefiting from their nanoscale dimensions and particle-like dynamic behavior, have opened new avenues for ultra-high-density and ultra-low-power neuromorphic computing, holding great promise for future in-memory computing architectures [43]. However, their practical development is still hindered by limited thermal stability, difficulties in precise control, and the lack of reliable experimental array demonstrations at the array level [44].

**Table 2.** The different functions of various devices used in neuromorphic computing.

| Device type | Typical mechanism | Synaptic functions | Neuron functions | Advantages | Limitations |
|---|---|---|---|---|---|
| STT MTJ [23,31] | Spin-transfer torque | binary/multi-level weight; LTP/LTD | M-P neuron | mature CMOS compatibility; low cost; high array density | write disturbance; low linearity; moderate speed; |
| SOT MTJ [27,37] | Spin-orbit torque | binary/multi-level weight; STDP; LTP/LTD | LIF neuron | ultra-fast switching; low write disturbance; good linearity; | high write current; complex heavy-metal stack; |
| Domain-wall MTJ [20,42] | Magnetic domain wall motion | binary/multi-level weight short/long-term memory | Sensory neuron, | multistable resistance; high weight resolution | domain wall pinning; low speed; low density; |
| Skyrmion MTJ [26,38] | Magnetic skyrmion nucleation/motion | binary/multi-level weight; STDP | LIF neuron | ultra-small size; ultra-low power; particle-like dynamics | poor stability; hard to control; mostly simulation; |

To address these limitations, the stability and controllability issues in domain wall and skyrmion systems can be mitigated by developing materials with gradient magnetic anisotropy or synthetic antiferromagnetic structures [45]. Furthermore, multi-field collaborative modulation mechanisms need to be further developed by integrating electrical, magnetic, thermal, and other stimuli to achieve novel plasticity rules that simultaneously offer high linearity, low power consumption, and high robustness. Finally, the maturation of large-scale heterogeneous integration technologies is crucial, which necessitates solving the challenge of efficient interfacing between MTJ devices and CMOS peripheral circuits to ultimately construct truly scalable and manufacturable full-hardware neuromorphic computing systems.

## 4. Spin neural network

Neuromorphic computing aims to use hardware to build a network to imitate the structure and calculation methods of biological neural networks, perform efficient data processing, and achieve cognitive and other functions [46]. Building hardware neural networks based on MTJs has been extensively studied in the past few years, and some progress has been made [8]. Currently, researchers have used MTJ neuromorphic devices to construct various networks such as ANNs, SNNs, and Recurrent Neural Networks (RNNs). A detailed overview of the current research status is provided below.

### *4.1. Artificial neural networks*

The magnetoresistance effect of MTJ devices endows them with the dual functionality of weight storage and input sensing, positioning them as promising candidates for the hardware implementation of ANNs. Specifically, the external magnetic fields can dynamically modulate the device conductance, which is subsequently encoded as the synaptic weight in the neural network. Concurrently, the voltage ($V$) applied across the MTJ serves as the input signal to the synapse. In accordance with Ohm's law, the output current ($I$) of a single MTJ synaptic device is given by $I = V \times G(H_{\text{eff}})$, where $G(H_{\text{eff}})$ represents the field-modulated conductance of the MTJ. When MTJ devices are arranged in a crossbar array, the total current accumulated at each output node corresponds to the dot product of the input vector and the weight

matrix, thereby enabling massively parallel information processing analogous to that observed in biological neural networks. In 2016, Zhang *et al.* constructed a full-spin ANN composed of three layers of fully connected feed-forward networks, using a cross array structure for inter-layer connection, and using composite synapses made of MTJs as intersection points [47], as shown in Figure 5a. The cross-point resistance represents the synaptic weight. Using an offline learning method, the trained synaptic weights were mapped to the device resistance MTJ. Through system-level simulation, it was confirmed that the network can realize the recognition of the MNIST handwriting dataset, and the recognition accuracy is about 90.85%. In 2022, Zhao *et al.* constructed an MTJ sensor cross array as shown in Figure 5b. They employed an external FPGA to perform gradient computation, implement BP backpropagation, and complete weight parameter updates. Finally, the functions of a fully connected classifier autoencoder and a convolutional neural network classifier were realized. The time for correct classification of one picture was less than 9 μs [48].

Although the feasibility of modulating MTJ conductance via magnetic fields has been preliminarily validated in small-scale arrays, studies indicate that for large-scale integrated arrays, individually addressing thousands of devices using magnetic fields poses severe challenges in terms of magnetic crosstalk and integration density [49]. To overcome these challenges, current mainstream hardware implementations predominantly adopt electrical addressing schemes, such as leveraging the SOT effect to achieve field-free writing [50].

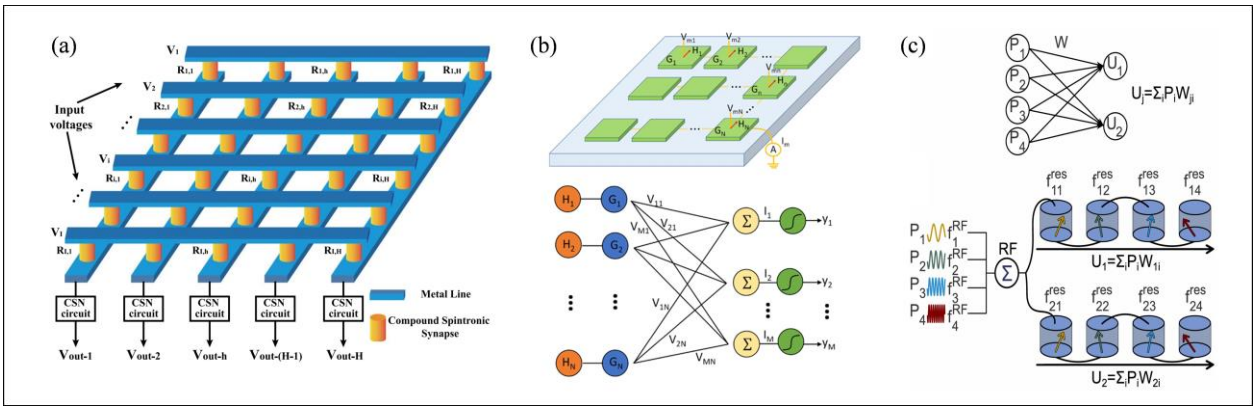


**Figure 5.** ANN composed of MTJ arrays. **(a)** Full-spin ANN [47]. Reprinted with permission. Copyright 2016 IEEE; **(b)** ANN classifiers based on MTJ array [48]. Reprinted with permission. Copyright 2023 IEEE; **(c)** ANN composed of RF-connected MTJ array [51]. Reprinted with permission. Copyright 2021 APS.

The spin diode effect of the STNO device allows the synaptic weight $W$ to be encoded by the difference between injected microwave signal frequency and the device's oscillation frequency. The rectified output voltage $V$ is then proportional to the product of the injected microwave power $P$. Leveraging this property, in 2021, Leroux *et al.* used spin nano-oscillators as artificial synapses to construct a fully connected network to realize the identification of radio frequency signals [51]. Based on the measured device characteristics and physical parameters, a simulation model was built to simulate the multiplication and accumulation operation of the ANN, and the classification of microwave coding input was realized as shown in Figure 5c. On this basis, a single-layer neural network was built to realize radio frequency signal classification of handwritten digits, with a maximum recognition accuracy of 99.40%.

Using an MTJ to build a cross array to realize a fully connected neural network in hardware is currently a promising solution for realizing commercial neuromorphic computing. The cross array based on the oscillation characteristics of the MTJ has lower energy consumption and a single node also has richer adjustability. Although the output power and stability of the spin nano-oscillator need to be further improved, this solution provides a microwave signal transmission method between network layers and provides a powerful solution for realizing low-power, large-scale neural network calculations.

### *4.2. Spiking neural networks*

SNNs are computational models inspired by biological nervous systems. MTJs serve as the core devices of SNN: they are not only used to simulate neuronal lateral inhibition and LIF neuron models through spin manipulation characteristics, thereby supporting perceptual functions such as simple image recognition [52], but also provide the hardware foundation for constructing cerebral cortex-like hierarchical sequential memory algorithms [53,54]. Realized via the current competition or magnetic coupling effect of MTJ arrays, this mechanism offers core support for the functional optimization of multi-scale simulations.

In 2016, Zhang *et al.* proposed a random spiking neuron circuit with an MTJ as the core, as shown in Figure 6a. Multiple MTJs were used in parallel to simulate single synaptic plasticity. Based on this, a two-layer fully connected SNN was constructed. The simplified random STDP algorithm and lateral suppression were used to achieve the recognition of MNIST, with a recognition accuracy of 91.27% [25]. In 2022, Romera *et al.* used STNO's injection phase-locking characteristics to simulate the synchronous binding characteristics of neurons in the brain, forming a single layer of multiple neurons to bind to continuous events and identify and distinguish timing [55], as shown in Figure 6b. In 2020, Zheng *et al.* used the synaptic-like short-term inhibition characteristics of the dynamic magnetization process of MTJs to construct a one-dimensional and two-dimensional Continuous Attractor Neural Network (CANN) [56], as shown in Figure 6d. This article proves that the use of a 2D CANN network composed of 27 × 40 MTJ neurons can realize the tracking and motion prediction of a rolling ping pong ball in a video. In contrast to conventional integrated circuit-based designs, this network architecture offers superior energy efficiency, making it particularly suitable for edge deployment in portable, low-power detection terminals. This learning paradigm can also be extended to antiferromagnetic devices. By exploiting the physical mechanism of nonlinear magnon scattering modulated by omnidirectional hopfion motion in antiferromagnets, researchers have constructed a single-device meta-learning neuromorphic system, which alleviates the limitations of hardwired connections and low connection density in traditional synaptic devices. It enables high-precision prediction of complex signals, achieving normalized root-mean-square error (NRMSE) values of 0.028 for periodic signals and 0.041 for Lorenz chaotic signals, while holding great potential for low power consumption and high stability [43].

Pulse Coupled Neural Network (PCNN) is a special branch of SNN, which simulates the working principle of the biological optic nerve. The neurons of PCNN have global coupling properties. The degree of coupling is adjusted by introducing inhibitory or excitatory signals. In 2018, Romera *et al.* proposed a two-layer hardware PCNN composed of STNO to realize the recognition of 7 vowel patterns [57], as shown in Figure 6c. The first layer works as the input, using 2 STNOs to encode 7 vowels. The second layer is the calculation layer. where the STNO's oscillation is adjusted by the DC input current. When

the STNO is coupled to the input signal, different frequency locking ranges are obtained according to the different possibilities of coupling. These locking ranges are used to represent different vowels. The accuracy of vowel recognition in the experiment was 89%, close to the maximum recognition rate of 94%. This solution provides a new path for future large-scale hardware neural networks.

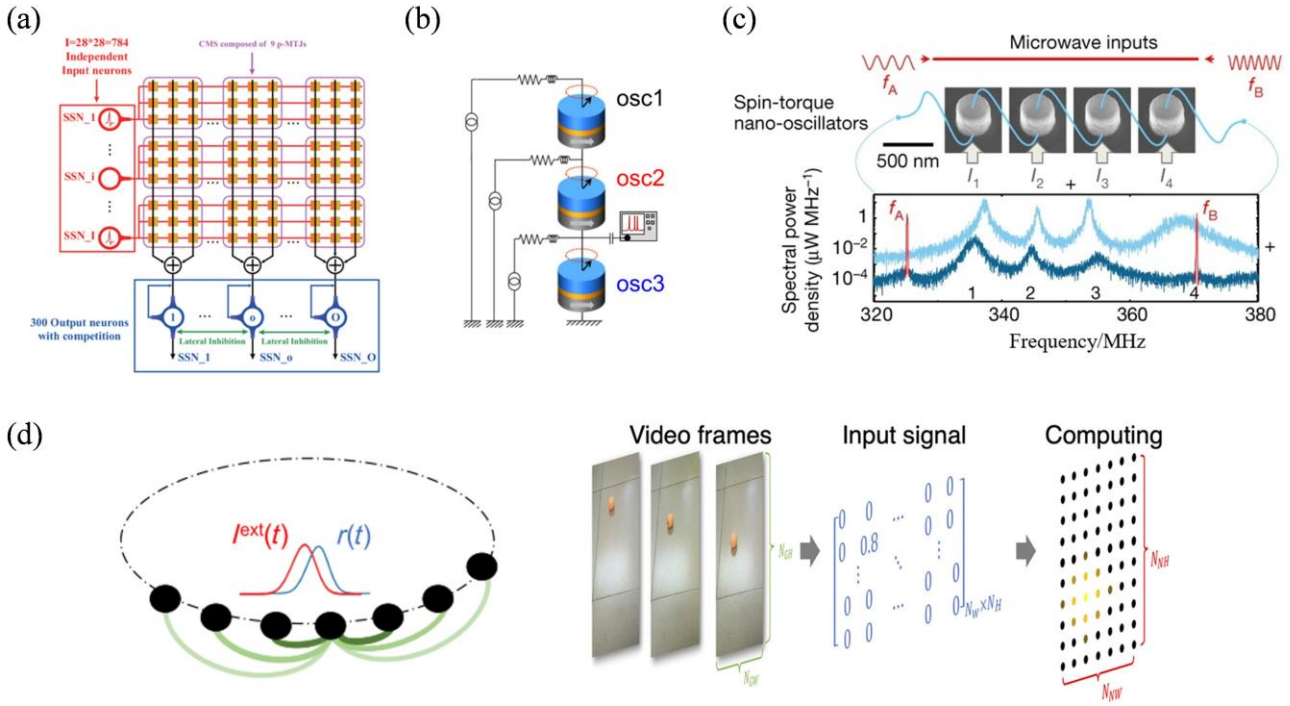


**Figure 6.** SNN composed of MTJ. **(a)** Stochastic impulse neural network [25]. Reprinted with permission. Copyright 2016 ACM; **(b)** STNO circuits for simulating associative memory neurons [55]. Reprinted with permission. Copyright 2022 Nature; **(c)** STNO-based pulse coupled neural network [57]. Reprinted with permission. Copyright 2018 Nature; **(d)** 2D CANN and schematic diagram of target tracking principle [56]. Reprinted with permission. Copyright 2020 APS.

### *4.3. Recurrent neural network*

RNN can capture long-term dependencies. It can remember previous input information and process inputs of any length, which makes it suitable for natural language processing, speech recognition, *etc.* RNN consists of an input layer, a hidden layer and an output layer. The hidden layer maintains a hidden state that carries information from previous time steps. MTJs have efficient parallel computing capabilities and storage capabilities. Building an RNN network based on MTJ neurons can achieve efficient and low-power computing. In 2020, Zheng *et al.* used 40 MTJs to form a RNN, and finally achieved the generation and recognition of periodic time series [58]. The network structure is shown in Figure 7a. The RNN was trained to simulate handwritten characters of the Chinese writing system. This kind of RNN based on MTJ can resist the noise of the input signal. At the same time, due to the low requirements on device consistency, it is expected to significantly improve the energy efficiency and integration density of neuromorphic devices.

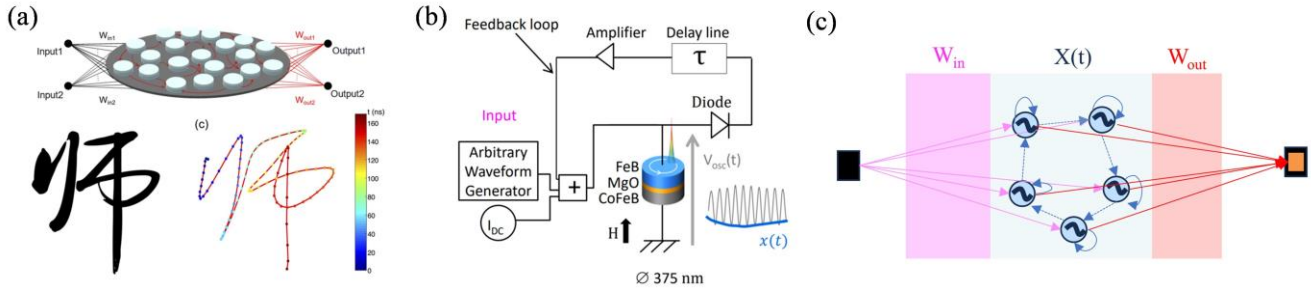


**Figure 7.** RNN composed of MTJ. **(a)** MTJ-based recurrent neural [58]. Reprinted with permission. Copyright 2020 AIP Publishing; **(b)** STNO neuron circuit based on voltage feedback [59]. Reprinted with permission. Copyright 2019 APS; **(c)** Schematic diagram of STNO-based reservoir computing [59]. Reprinted with permission. Copyright 2019 APS.

Reservoir Computing (RC) is derived from RNN. This kind of network can introduce rich nonlinear dynamics through randomly connected reservoir pools (also called dynamical systems), which can perform high-dimensional nonlinear mapping of input data. At the same time, since the structure of the reserve pool is fixed, only the weights of the output layer need to be trained. This greatly simplifies the training process and reduces the complexity and computational cost of parameter adjustment. Based on the nonlinear characteristics of MTJs, researchers have carried out research on MTJ-based RC.

In 2019, Riou. *et al.* used the short-term memory of STNO to increase external memory through a time-delay feedback loop, as shown in Figure 7b. Based on the STNO devices, they constructed a RC by using time-sharing multiplexing of a single device (Figure 7c). The input is projected to a higher dimension in time, and the memory of the device is used to enhance its efficiency in solving pattern recognition tasks. Simulation shows that after adding a feedback loop, the network accuracy rate increases from 89.2% to 99.84% [59]. Furthermore, in order to achieve the best recognition performance, the device oscillation frequency and phase can be adjusted by applying different bias currents or external magnetic fields. This work brings a new path to solve complex sequence recognition. The use of time-division multiplexing of a single device can reduce the overall network energy consumption and improve system integration [60]. In 2022, Kaonao *et al.* studied the RC of spin torque oscillator arrays, their simulation result shows that functions including short-term memory and parity checking can be realized by utilizing the synchronous oscillation characteristics of the MTJ array [61]. Furthermore, simulations demonstrate that increasing the number of STNOs in the array improves network performance. RC offers lower implementation complexity and power consumption, making it better aligned with the requirements of practical applications. It is therefore considered one of the most promising approaches for achieving on-chip training and real-time recognition [62]. Furthermore, the electrical detection of movable skyrmions via time-varying TMR signals in racetrack-like devices [63], an achievement realized by integrating skyrmion-hosting magnetic multilayers with MTJs, and the electrical nucleation and annihilation of individual skyrmions within MTJs via the voltage-controlled magnetic anisotropy (VCMA) effect [44] have collectively endowed skyrmion-based devices with an intrinsic compatibility for RC.

To systematically summarize the performance of spin-based neuromorphic computing systems in practical applications, Table 3 systematically organizes the application details of different magnetic devices in various neural networks, covering key parameters, task objectives, and performance metrics. As can be seen from the data in the table, neuromorphic computing systems centered on MTJs and

STNOs exhibit significant advantages in tasks such as handwritten digit recognition and signal processing. Through reasonable network structure configuration (e.g., 784-dimensional input encoding and optimized hidden-layer nodes), efficient classification on the MNIST dataset is achieved, with classification accuracy stably above 85% and exceeding 90% in some scenarios [19,25,57,59].

**Table 3.** Performance comparison of neuromorphic computing systems based on different spin-device types.

| Device Type | Neural Network Type | Network Scale | Task | Performance |
|---|---|---|---|---|
| **MTJs** | ANN [19] | Hidden layer: 64 × 64 1T-1MTJ array | MNIST handwritten digit recognition | Classification accuracy of 97%–98%<br>Computational energy efficiency of 10–20 TOPS/W |
| | ANN [48] | Hidden layer: 3 × 3 p-MTJ array | Magnetic letter (Z, Y, H, L) recognition | 100% accuracy after 52 epochs<br>< 9 μs classification time per image |
| | SNN [25] | Input layer: 784 nodes<br>Hidden layer: Synapses with 9 CMS<br>Output layer: 300 neurons | MNIST handwritten digit recognition | 91.27% accuracy (using simplified stochastic STDP algorithm and lateral inhibition) |
| | RNN [56] | 1D CANN: 20 MTJs<br>2D CANN: 1128 MTJs | Multi-object tracking | 2D CANN with 21 s × 21 neurons can simultaneously track two motion signals (circular + square trajectories) via simulation |
| **STNOs** | ANN [51] | Hidden layer:10 resonator chains,<br>each with 784 STNOs | MNIST handwritten digit recognition | 99.40% accuracy; Minimum power consumption of 8 mW |
| | SNN [55] | Hidden layer: 3 MTJs | Continuous event binding, temporal recognition and discrimination | Mimics the synchronous binding property of biological neurons to distinguish temporal signals |
| | RNN [57] | Input layer: 2 STNOs | 7 vowel pattern recognition | 89% accuracy |
| | RC [59] | Reservoir layer: Single device | Waveform classification (sine & cosine) | 99.84% accuracy |
| **Stochastic MTJs** | ANN [64] | Input layer: 784 nodes<br>Hidden layer: 1–2 layers (100–200 nodes)<br>Output layer: 10 nodes | MNIST handwritten digit recognition<br>CIFAR-10 image classification | 98% accuracy on MNIST<br>85% accuracy on CIFAR-10 |
| | SNN [33] | Hidden layer: 10–20 MTJs per feature dimension | Unsupervised clustering on Iris dataset | 95% clustering accuracy; Remains above 85% when device variation is ±20% |

**Table 3.** *Cont.*

| Device Type | Neural Network Type | Network Scale | Task | Performance |
|---|---|---|---|---|
| **Stochastic MTJs** | RNN [65] | Hidden layer: 64 × 10 MTJ array | User preference memory and prediction for recommendation systems | 96.08% accuracy; |
| | RC [66] | Reservoir layer: 32 MTJ | Square wave signal processing and reconstruction<br>Sine wave signal prediction | Distortion-free reconstruction of input square waves; High coincidence degree with predicted sine wave trajectories; |
| Domain-wall MTJs - | ANN [67] | Hidden layer: 256 Domain-wall MTJ synapses; 16 Domain-wall MTJ neurons | Fashion-MNIST handwritten digit recognition | 89% classification accuracy; Maximum operating frequency of 20 MHz; Energy consumption of only 508 fJ/spike; |
| | SNN [68] | Input layer: 784 nodes<br>Hidden layer: 128 Domain-wall MTJ neurons<br>Output layer: 10 nodes | Fashion-MNIST handwritten digit recognition | 87% accuracy; |
| | RNN [58] | Input layer: 8 nodes<br>Recurrent layer: 40 Domain-wall MTJ neurons<br>Output layer: 1 node | Periodic temporal signal generation and recognition | 85% accuracy with 40 neurons; 92% accuracy when expanded to 60 neurons; |
| | ANN [69] | Input layer: 16 nodes<br>Synaptic layer: 16 × 16 Skyrmion array<br>Output layer: 10 nodes | MNIST handwritten digit recognition | 89% classification accuracy (verified by simulation); |
| **SkyrmionMTJs** | SNN [70] | Input layer: 576 nodes<br>Hidden layer: 600 Skyrmion neurons<br>Output layer: 10 nodes | MNIST handwritten digit recognition | 91% accuracy; |
| | RNN [71] | Input layer: 10,000 nodes<br>Recurrent layer: 512 recurrent neurons<br>Output layer: 3 nodes | Temporal dynamic process classification and learning | Long-term temporal dependence captured by recurrent network; Automatic recognition of ultrafast skyrmion dynamics; |
| | RC [72] | Input layer: 784 nodes<br>Reservoir layer: 1 device<br>Output layer: 10 nodes | MNIST handwritten digit recognition | 94.7% accuracy; |

Among these devices, MTJs show outstanding performance in low-power applications, with greatly improved computing energy efficiency (TOPS/W) compared with conventional CMOS circuits, and their response speed can be further optimized through timing control. STNOs present strong anti-interference capability in dynamic signal processing, especially in tasks such as multi-object tracking and waveform classification, where efficient resource utilization is realized via time-division multiplexing.

Notably, neuromorphic systems based on domain-wall motion maintain high recognition accuracy (e.g., over 90% for MNIST classification) while effectively reducing hardware complexity, providing a feasible route for the engineering implementation of neuromorphic computing. These results fully demonstrate that spin-based neuromorphic computing systems possess remarkable advantages in task

adaptability, power consumption control, and stability, thus offering important references for the subsequent integration and optimization of neuromorphic chips.

## 5. Conclusion

In summary, MTJs emerged as one of the most promising devices for hardware-efficient neuromorphic computation, owing to their intrinsic nonlinearity, stochastic switching behavior, multi-physics field tunability and compatibility with CMOS processes. This paper reviews the recent progress of MTJ devices in neuromorphic computing from three perspectives: (i) The fundamental physical mechanisms of MTJ devices, including TMR, STT, SOT and magnetization dynamics, have been reviewed in detail. Notably, fully epitaxial MTJs fabricated on 8-inch silicon wafers have achieved a high MR ratio exceeding 240% at room temperature by using a B2-type Ni-Al seed layer and a spinel-type Mg-Al-O tunnel barrier, which provides a solid foundation for high-performance neuromorphic hardware [73]. (ii) The steady magnetization switching state, oscillatory output voltage and dynamic flipping process of MTJ devices have been exploited to emulate synaptic weights and plasticity rules. Meanwhile, different kinds of neuron models have been achieved by using the random flipping and spin oscillation characteristics. For instance, stacked perpendicular MTJs with a diameter of 50 nm enable four-level operation via low-voltage switching (< 0.5 V), offering a scalable solution for multi-level synaptic weight encoding [74]. Additionally, hybrid neural network-based MTJ modeling frameworks integrating GNN and DNN have been proposed to precisely approximate cross-level coupled physical processes, while stable diffusion (SD) models reproduce production-line parameter variations, bridging the gap between idealized simulations and real hardware performance [75]. (iii) A broad range of neuromorphic computing studies based on MTJ devices has already been conducted, spanning from analog ANNs to SNNs and RNNs. These MTJ-enabled networks have demonstrated the capability to perform tasks such as image and speech recognition. Scaling studies of in-plane and perpendicular MTJs from 65 nm to 8 nm have shown that in-plane STT-MRAM outperforms SRAM from the 15 nm node (with TMR > 200% and aggressive assist schemes), verifying the feasibility of MTJ-based high-density neuromorphic hardware [76].

Although different types of MTJ devices have been validated for neuromorphic computing applications, various challenges still need to be overcome in how to promote the practical application and sustainable development of this technology. We provide a detailed discussion from two perspectives.

First, from the device perspective, existing MTJ synapses and neurons often rely on simplified or idealized models that do not fully capture device nonideality, causing the difficulty to bridge the gap between simulated and hardware performance. Besides, the TMR values should be higher to ensure sufficient sensing margin and mitigate read disturbances in MTJ crossbar arrays, particularly in large-scale systems. At the same time, the preparation process of nanoscale MTJs is more complicated. These limitations, together with variability of different devices, hinder the realization of robust and scalable MTJ-based neuromorphic computing. For example, perpendicular MTJs face severe write performance degradation beyond the 15 nm node due to constant critical switching current ($I_0$) and extremely low required RA values (< 0.2 Ω·μm²), leading to reliability issues in thin tunneling barriers [76]. Moreover, despite theoretical predictions of ultra-high TMR (100,000%) for graphene-based MTJs, experimental values remain far lower, highlighting the need for materials innovation [77].

Second, at the network level, most current MTJ-based hardware neural network demonstrations operate on small-scale networks and rely on peripheral CMOS circuitry for critical functions. The hybrid MTJ–CMOS systems face challenges in interconnect density and signal conversion overhead. Besides, most existing research still focuses on implementing conventional neural network trained with mature BP algorithms. However, such models and learning rules are not intrinsically aligned with the physical characteristics and operational constraints of MTJ-based neuromorphic hardware. For example, the BP algorithm has problems such as redundant calculations and global error propagation. These issues substantially increase the training cost when implemented on MTJ-based hardware. As a result, directly mapping the mature networks onto MTJ arrays often leads to degraded performance, increased overhead of the device's native computational advantages.

To address the aforementioned challenges, several research directions merit deeper investigation. On the device side, the interface optimization, materials innovation and improvement of fabrication process are essential to reduce variability, enhance endurance, and improve the TMR values. Recently, some researchers pointed out that an MTJ with graphene as a barrier layer has a theoretical TMR value of 100,000%. However, the currently reported experimental value of the magnetoresistance change rate of graphene MTJ is still far lower than the theoretical prediction value [69,78]. The development of fully epitaxial MTJs on silicon wafers and stacked MLC MTJs provides effective pathways for improving TMR and scalability [73,74]. Additionally, production-line level modeling frameworks (e.g., GNN+DNN+SD) can accurately predict parameter variations, facilitating robust circuit design [75].

At the network level, the integration of MTJ devices into crossbar or 3D stacked architectures represents a promising way for achieving high-density and low-latency computation. Moreover, comprehensive hardware-algorithm co-design frameworks are needed to accommodate device stochasticity, exploit inherent nonlinearity, and support online learning. For example, the forward-forward algorithm has been proposed as a promising candidate for training neural networks in physical systems, though its development is still at an early stage and it has not yet been shown to outperform backpropagation [79]. Besides, we noticed that the rich intrinsic nonlinear responses of MTJ devices align well with the nonlinear basis functions. Therefore, it may be a highly promising research direction to integrate MTJs with Kolmogorov–Arnold Networks (KANs), which represent functions through adaptive nonlinear operators [80]. For optical-electrical MTJs, leveraging frequency multiplexing of laser signals can enable parallel processing, and cascading multiple bTMS-based MTJ layers supports deeper neural networks with enhanced expressive power [81].

Overall, MTJ-driven neuromorphic hardware holds substantial potential. And continued efforts across materials science, fabrication process, circuit design, and hardware-aware algorithms will be key to unlocking its full capability.

## Data availability statement

No supplementary or additional data were generated in this study.

## Declaration of generative AI and AI-assisted technologies

During the preparation of this manuscript, the authors used generative AI tools only to improve language and readability. Specifically, the authors used Doubao, DeepSeek, *etc.* for language polishing and limited drafting of partial sections. The authors take full responsibility for the content of the manuscript.

## Acknowledgments

Funding: this work was supported by the National Key R&D Program of China (Grant No. 2023YFB2407700), the National Natural Science Foundation of China (Grant Nos. 62004223, 62201599, and 62304259), the Science and Technology Innovation Program of Hunan Province (Grant No. 2022RC1094) and Innovation Research Foundation of National University of Defense Technology.

## Authors' contribution

Liyuan Yang: writing—original draft preparation; Mengchun Pan: supervision and funding acquisition; Peisen Li: writing—review and funding acquisition; Miaosen Liu: investigation; Minhui Ji: writing—review and editing. All authors have read and agreed to the published version of the manuscript.

## Conflicts of interest

The authors declare that there are no potential conflicts of interest.

## References

[1] Dentella V, Günther F, Leivada E. Language *in vivo vs.* in silico: size matters but larger language models still do not comprehend language on a par with humans due to impenetrable semantic reference. *PLoS One* 2025, 20(7):e0327794.

[2] Levy W, Calvert V. Communication consumes 35 times more energy than computation in the human cortex, but both costs are needed to predict synapse number. *Proc. Natl. Acad. Sci. U. S. A.* 2021, 118(18):1–12.

[3] Merolla P, Arthur J, Alvarez-Icaza R, Cassidy A, Sawada J, *et al.* A million spiking-neuron integrated circuit with a scalable communication network and interface. *Science* 2014, 345(6197):668–673.

[4] Benjamin B, Gao P, McQuinn E, Choudhary S, Chandrasekaran A, *et al.* Neurogrid: a mixed-analog-digital multichip system for large-scale neural simulations. *Proc. IEEE* 2014, 102(5):699–716.

[5] Zhang W, Yao P, Gao B, Liu Q, Wu D, *et al.* Edge learning using a fully integrated neuro-inspired memristor chip. *Science* 2023, 381(6663):1205–1211.

[6] Syed G, Le Gallo M, Sebastian A. Phase-change memory for in-memory computing. *Chem. Rev.* 2025, 125(11):5163–5194.

[7] Oh S, Hwang H, Yoo I. Ferroelectric materials for neuromorphic computing. *APL Mater.* 2019, 7(9):091109.

[8] Grollier J, Querlioz D, Camsari K, Everschor-Sitte K, Fukami S, *et al.* Neuromorphic spintronics. *Nat. Electron.* 2020, 3:360–370.

[9] Julliere M. Tunneling between ferromagnetic films. *Phys. Lett. A* 1975, 54(3):225–226.

[10] Slonczewski J. Conductance and exchange coupling of two ferromagnets separated by a tunneling barrier. *Phys. Rev. B* 1989, 39(10):6995–7002.
[11] Slonczewski J. Current-driven excitation of magnetic multilayers. *J. Magn. Magn. Mater.* 1996, 159(1–2):L1–L7.
[12] Ament S, Rangarajan N, Parthasarathy A, Rakheja S. Solving the stochastic landau-lifshitz-gilbert-slonczewski equation for monodomain nanomagnets: a survey and analysis of numerical techniques. *arXiv* 2017, arXiv:1607.04596.
[13] Zeng Z, Finocchio G, Jiang H. Spin transfer nano-oscillators. *Nanoscale* 2013, 5(6):2219–2231.
[14] Brown WF Jr. Thermal fluctuations of a single-domain particle. *Phys. Rev.* 1963, 130(5):1677–1686.
[15] Rippard W, Heindl R, Pufall M, Russek S, Kos A. Thermal relaxation rates of magnetic nanoparticles in the presence of magnetic fields and spin-transfer effects. *Phys. Rev. B* 2011, 84(6):064439.
[16] Sporns O, Tononi G, Kötter R. The human connectome: a structural description of the human brain. *PLoS Comput. Biol.* 2005, 1(4):e42.
[17] Huang F, Sun X, Shi Y, Pan L. Flexible ionic-gel synapse devices and their applications in neuromorphic system. *FlexMat.* 2025, 2(1):30–54.
[18] Kim K, Song M, Hwang H, Hwang S, Kim H. A comprehensive review of advanced trends: from artificial synapses to neuromorphic systems with consideration of non-ideal effects. *Front Neurosci.* 2024, 18:1279708.
[19] Jung S, Lee H, Myung S, Kim H, Yoon SK, *et al.* A crossbar array of magnetoresistive memory devices for in-memory computing. *Nature* 2022, 601(7892):211–216.
[20] Cai J, Fang B, Wang C, Zeng Z. Multilevel storage device based on domain-wall motion in a magnetic tunnel junction. *Appl. Phys. Lett.* 2017, 111(18):182410.
[21] Raymenants E, Vaysset A, Wan D, Manfrini M, Zografos O, *et al.* Chain of magnetic tunnel junctions as a spintronic memristor. *J. Appl. Phys.* 2018, 124(15):152116.
[22] Ji M, Yang L, Pan M, Zhang X, Wang J, *et al.* In-sensor nonlinear convolutional processing based on hybrid MTJ/CMOS arrays. *Digit. Signal Process.* 2024, 147:104412.
[23] Sengupta A, Roy K. Short-term plasticity and long-term potentiation in magnetic tunnel junctions: towards volatile synapses. *Phys. Rev. Appl.* 2016, 5(2):024012.
[24] Prasad N, Pramanik T, Banerjee S, Register L. Realizing both short- and long-term memory within a single magnetic tunnel junction based synapse. *J. Appl. Phys.* 2020, 127(9):093904.
[25] Zhang D, Zeng L, Zhang Y, Zhao W, Klein J. Stochastic spintronic device based synapses and spiking neurons for neuromorphic computing. In *Proceedings of the 2016 IEEE/ACM International Symposium on Nanoscale Architectures (NANOARCH)*, Beijing, China, July 18–20, 2016, pp. 173–178.
[26] Lone A, Fariborzi H. Skyrmion-magnetic tunnel junction synapse with long-term and short-term plasticity for neuromorphic computing. *IEEE Trans. Electron Devices* 2023, 70(1):371–378.
[27] Cao Z, Zhang S, Hou J, Duan W, You L. All-spin artificial neural network based on spin–orbit torque-induced magnetization switching. *IEEE Trans. Electron Devices* 2023, 70(12):6336–6340.
[28] Vadde V, Muralidharan B, Sharma A. Power efficient relu design for neuromorphic computing using spin hall effect. *J. Phys. D: Appl. Phys.* 2023, 56(41):415001.
[29] Wood IK. *Neuroscience: Exploring The Brain*, 1st ed. Philadelphia: Lippincott Williams & Wilkins, 1996. pp. 377–379.

[30] Purves D, Augustine GJ, Fitzpatrick D, Hall WC, LaMantia AS, *et al*. *Neuroscience*, 6th ed. New York: Oxford University Press, 2018. pp. 115–130.

[31] Suh D, Bae G, Oh H, Park W. Neural coding using telegraphic switching of magnetic tunnel junctions. *J. Appl. Phys.* 2015, 117(17):17D714.

[32] Ribeiro S, Brunel N, Hakim V. Clustering of neural activity: a design principle for population codes. *Front. Comput. Neurosci*. 2020, 14:20.

[33] Zhang Y, Li J, Wang X, Zeng Z, Yuan J, *et al.* Implementation of unsupervised clustering based on population coding of magnetic tunnel junctions. *Acta Phys. Sin.* 2022, 71(14):148506.

[34] Sharad M, Fong X, Roy K. Magnetic tunnel junction mimics stochastic cortical spiking neurons. *Sci Rep*. 2016, 6:30039.

[35] Marković D, Daniels MW, Sethi P, Kent A, Stiles M, *et al.* Easy-plane spin hall nano-oscillators as spiking neurons for neuromorphic computing. *Phys. Rev. B* 2022, 105(1):014411.

[36] Wang D, Lin H, Xu N, Liu L, Lin H, *et al.* Synergy of spin-orbit torque and built-in field in magnetic tunnel junctions with tilted magnetic anisotropy: toward tunable and reliable spintronic neurons. *Adv. Sci.* 2022, 9(30):2203006.

[37] Wang C, Lee C, Roy K. Noise resilient leaky integrate-and-fire neurons based on multi-domain spintronic devices. *Sci. Rep*. 2022, 12:8361.

[38] Yu Z, Shen M, Zeng Z. Voltage-controlled skyrmion-based nanodevices for neuromorphic computing using a synthetic antiferromagnet. *Nanoscale Adv.* 2020, 2(3):1309–1317.

[39] Cai B, He Y, Xin Y, Yuan Z, Zhang X, *et al.* Unconventional computing based on magnetic tunnel junction. *Appl. Phys. A* 2023, 129(4):236.

[40] Sato N, Allen G, Benson W, Buford B, Chakraborty A, *et al*. CMOS Compatible process integration of SOT-MRAM with heavy-metal bi-layer bottom electrode and 10 ns field-free SOT switching with STT assist. In *Proceedings of the 2020 IEEE Symposium on VLSI Technology*, Honolulu, USA, June 16–19, 2020, pp. 1–2.

[41] Van Beek S, Cai K, Rao S, Jayakumar G, Couet S, *et al*. MTJ degradation in SOT-MRAM by self-heating-induced diffusion. In *Proceedings of the 2022 IEEE International Reliability Physics Symposium (IRPS)*, Dallas, USA, March 27–31, 2022, pp. 4A.2–1–4A.2–4.

[42] Kaur G, Pramanik T. Comparison of pinning potentials, depinning currents and scalability for domain wall-based synapses with various pinning structures. *J. Magn. Magn. Mater.* 2025, 629:173280.

[43] Zhang Z, Lin K, Zhang Y, Bournel A, Xia K, *et al.* Magnon scattering modulated by omnidirectional hopfion motion in antiferromagnets for meta-learning. *Sci. Adv.* 2023, 9:eade7439.

[44] Urrestarazu Larrañaga J, Sisodia N, Guedas R, Pham V, Manici I, *et al.* Electrical detection and nucleation of a magnetic skyrmion in a magnetic tunnel junction observed via operando magnetic microscopy. *Nano Lett.* 2024, 24(12):3557–3565.

[45] Leonard T, Zogbi N, Liu S, Rogers W, Bennett C, *et al.* Shape anisotropy-dependent leaking in magnetic neurons for bio-mimetic neuromorphic computing. *ACS Nano* 2025, 19(3):3470–3477.

[46] Roy K, Jaiswal A, Panda P. Towards spike-based machine intelligence with neuromorphic computing. *Nature* 2019, 575(7784):607–617.

[47] Zhang D, Zeng L, Cao K, Wang M, Peng S, *et al.* All spin artificial neural networks based on compound spintronic synapse and neuron. *IEEE Trans. Biomed. Circuits Syst.* 2016, 10(4):828–836.

[48] Zhao G, Peng Y, Wang Y, Wan C, Liu X, *et al*. Computing resistance-style image sensors for artificial neural networks. *IEEE Internet Things J.* 2023, 10(6):4985–4997.

[49] Zhang W, Hao Q, Xiao G. Low-frequency noise in serial arrays of MgO-based magnetic tunnel junctions. *Phys. Rev. B* 2011, 84(9):094446.

[50] Yang T, Yang M, Zhao L, Gao J, Xiang Q, *et al*. Field-free deterministic writing of spin-orbit torque magnetic tunneling junction by unipolar current. *IEEE Electron Device Lett.* 2022, 43(5):709–712.

[51] Leroux N, Marković D, Martin E, Petrisor T, Querlioz D, *et al.* Radio-frequency multiply-and-accumulate operations with spintronic synapses. *Phys. Rev. Appl.* 2021, 15(3):034067.

[52] Liu H, Ohsawa T. A binarized spiking neural network based on autoreset LIF neurons and large signal synapses using STT-MTJs. *Jpn. J. Appl. Phys.* 2023, 62(4):044501.

[53] Li S, Teng Z, Jia S, Wang Z, Cao K, *et al.* Scalable and energy-efficient on-device SNNs enabled by magnetic tunnel junctions. In *Proceedings of the 2025 IEEE 36th Magnetic Recording Conference (TMRC)*, Sendai, Japan, July 28–30, 2025.

[54] Cui C, Akinola O, Hassan N, Bennett C, Marinella M, *et al.* Maximized lateral inhibition in paired magnetic domain wall racetracks for neuromorphic computing. *Nanotechnology* 2020, 31(29):294001.

[55] Romera M, Talatchian P, Tsunegi S, Yakushiji K, Fukushima A, *et al.* Binding events through the mutual synchronization of spintronic nano-neurons. *Nat. Commun.* 2022, 13(1):883.

[56] Zheng Q, Mi Y, Zhu X, Yuan Z, Xia K. Anticipative tracking with the short-term synaptic plasticity of spintronic devices. *Phys. Rev. Appl.* 2020, 14(4):044060.

[57] Romera M, Talatchian P, Tsunegi S, Abreu Araujo F, Cros V, *et al.* Vowel recognition with four coupled spin-torque nano-oscillators. *Nature* 2018, 563(7730):230–234.

[58] Zheng Q, Zhu X, Mi Y, Yuan Z, Xia K. Recurrent neural networks made of magnetic tunnel junctions. *AIP Adv.* 2020, 10(2):025116.

[59] Riou M, Torrejon J, Garitaine B, Araujo FA, Bortolotti P, *et al.* Temporal pattern recognition with delayed feedback spin-torque nano-oscillators. *Phys. Rev. Appl.* 2019, 12(2):024049.

[60] Zhong Y, Tang J, Li X, Gao B, Qian H, *et al.* Dynamic memristor-based reservoir computing for high-efficiency temporal signal processing. *Nat. Commun.* 2021, 12(1):408.

[61] Kanao T, Suto H, Mizushima K, Goto H, Tanamoto T, *et al.* Reservoir computing on spin-torque oscillator array. *Phys. Rev. Appl.* 2019, 12(2):024052.

[62] Akashi N, Yamaguchi T, Tsunegi S, Taniguch T, Nishida M, *et al.* Input-driven bifurcations and information processing capacity in spintronics reservoirs. *Phys. Rev. Res.* 2020, 2(4):043303.

[63] Zhao M, Chen A, Huang P, Liu C, Shen L, *et al.* Electrical detection of mobile skyrmions with 100% tunneling magnetoresistance in a racetrack-like device. *npj Quantum Mater.* 2024, 9(1):50.

[64] Sabyasachi S, Misba W, Shao Y, Amiri P, Atulasimha J. Quantized artificial neural networks implemented with spintronic stochastic computing. *arXiv* 2025, arXiv:2504.06414.

[65] Ye X, Duan C, Cao Z, Wang Z, You L. Construction of recommendation system based on spin-orbit torque random binary stochastic neurons. *Science Bulletin.* 2025, 70(13):1929–1936.

[66] Ganguly S, Camsari KY, Ghosh AW. Analog signal processing using stochastic magnets. *IEEE Access* 2021, 9:92640–92650.

[67] Liu L, Wang D, Wang D, Sun Y, Lin H, *et al.* Domain wall magnetic tunnel junction-based artificial synapses and neurons for all-spin neuromorphic hardware. *Nat. Commun.* 2024, 15(1):4534.

[68] Leonard T, Liu S, Jin H, Incorvia J. Stochastic domain wall-magnetic tunnel junction artificial neurons for noise-resilient spiking neural networks. *Appl. Phys. Lett.* 2023, 122(26):262406.

[69] Song K, Jeong J, Pan B, Zhang X, Xia J, *et al.* Skyrmion-based artificial synapses for neuromorphic computing. *Nat. Electron.* 2020, 3:148–155.

[70] Yang S, Moon K, Ju T, Son J, Kim T, *et al.* Magnetic skyrmion neurons with homeostasis for spiking neural networks. *ACS Nano* 2026, 20(1):240–247.

[71] Deviatov A, Iakovlev I, Mazurenko V. Recurrent network classifier for ultrafast skyrmion dynamics. *Phys. Rev. Appl.* 2019, 12(5):054026.

[72] Yokouchi T, Sugimoto S, Rana B, Seki S, Ogawa N, *et al.* Pattern recognition with neuromorphic computing using magnetic field-induced dynamics of skyrmions. *Sci. Adv.* 2022, 8(39):eabq5652.

[73] Yakushiji K, Sugihara A, Nakano T, Yuasa S. Fully epitaxial magnetic tunnel junction on a silicon wafer. *Appl. Phys. Lett.* 2019, 115(20):202403.

[74] Aoki M, Noshiro H, Tsunoda K, Iba Y, Hatada A, *et al.* Novel highly scalable multi-level cell for STT-MRAM with stacked perpendicular MTJs. In *Proceedings of the 2013 Symposium on VLSI Technology*, Kyoto, Japan, June 11–13, 2013, pp. T134–T135.

[75] Zhang Z, Lin K, Cao K, Wang J, Yang J, *et al*. A production line level MTJ modeling framework: integrating physical mechanisms, experimental data and manufacturing variation. In *Proceedings of the 2024 IEEE International Electron Devices Meeting (IEDM)*, San Francisco, USA, 2024, pp. 1–4.

[76] Chun K, Zhao H, Harms J, Kim T, Wang J, *et al.* A scaling roadmap and performance evaluation of in-plane and perpendicular MTJ based STT-MRAMs for high-density cache memory. *IEEE J. Solid-State Circuits.* 2013, 48(2):598–610.

[77] Yan Z, Xiao J, Zhang X, Fang C, Xu X. Giant tunneling magnetoresistance in Mn-and V-intercalated Graphene/h-BN based van der waals magnetic tunnel junctions. *Adv. Funct. Mater.* 2026, 36(15):11719.

[78] Karpan V, Khomyakov P, Starikov A, Giovannetti G, Zwierzycki M, *et al.* Theoretical prediction of perfect spin filtering at interfaces between close-packed surfaces of Ni or Co and graphite or graphene. *Phys. Rev. B* 2008, 78(19):195419.

[79] Hinton G. The forward-forward algorithm: some preliminary investigations. *arXiv* 2022, arXiv:2212.13345.

[80] Liu Z, Wang Y, Vaidya S, Ruehle F, Halverson J, *et al.* KAN: kolmogorov-arnold networks. *arXiv* 2024, arXiv:2404.19756.

[81] Oberbauer F, Winkel T, Böhnert T, Wanjura C, Claro M, *et al.* Magnetic tunnel junctions driven by hybrid optical-electrical signals as a flexible neuromorphic computing platform. *Commun. Phys.* 2025, 8(1):329.